Linear magnetoresistance in a topological insulator Ru_2Sn_3 Ⓕ

Y. Shiomi and E. Saitoh

COLLECTIONS

Ⓕ This paper was selected as Featured

open access

View Online   Export Citation   CrossMark

ARTICLES YOU MAY BE INTERESTED IN

Linear positive and negative magnetoresistance in topological insulator Bi_2Se_3 flakes
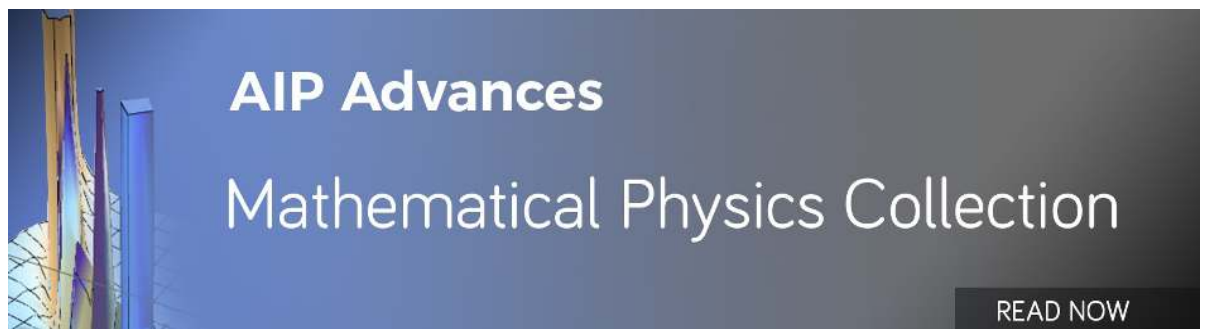Applied Physics Letters **113**, 113503 (2018); https://doi.org/10.1063/1.5044686

Linear magnetoresistance in topological insulator thin films: Quantum phase coherence effects at high temperatures
Applied Physics Letters **102**, 012102 (2013); https://doi.org/10.1063/1.4773207

Large anomalous Hall effect in ferromagnetic Weyl semimetal candidate PrAlGe
APL Materials **7**, 051110 (2019); https://doi.org/10.1063/1.5090795

AIP Advances

Mathematical Physics Collection

READ NOW

7, 035011

Linear magnetoresistance in a topological insulator Ru₂Sn₃

Y. Shiomi[1] and E. Saitoh[1,2,3]

[1]*Institute for Materials Research, Tohoku University, Sendai 980-8577, Japan*
[2]*WPI Advanced Institute for Materials Research, Tohoku University, Sendai 980-8577, Japan*
[3]*Advanced Science Research Center, Japan Atomic Energy Agency, Tokai 319-1195, Japan*

We have studied magnetotransport properties of a topological insulator material Ru_2Sn_3. Bulk single crystals of Ru_2Sn_3 were grown by a Bi flux method. The resistivity is semiconducting at high temperatures above 160 K, while it becomes metallic below 160 K. Nonlinear field dependence of Hall resistivity in the metallic region shows conduction of multiple carriers at low temperatures. In the high-temperature semiconducting region, magnetoresistance exhibits a conventional quadratic magnetic-field dependence. In the low-temperature metallic region, however, high-field magnetoresistance is clearly linear with magnetic fields, signaling a linear dispersion in the low-temperature electronic structure. Small changes in the magnetoresistance magnitude with respect to the magnetic field angle indicate that bulk electron carriers are responsible mainly for the observed linear magnetoresistance. © *2017 Author(s). All article content, except where otherwise noted, is licensed under a Creative Commons Attribution (CC BY) license (http://creativecommons.org/licenses/by/4.0/).* [http://dx.doi.org/10.1063/1.4978773]

Dirac fermion systems have recently attracted much attention in spintronics,[1] because of their potential high efficiency in the interconversion between spin currents and charge currents. One of the most prominent examples of Dirac fermion systems is topological insulators (TIs).[2–4] In TIs, strong spin-orbit coupling opens a charge gap in the bulk states, but 2D Dirac fermion systems appear on the surfaces. Dirac fermions form a Dirac cone in the band structure near the Fermi level; transport phenomena are governed by the Dirac fermions if the bulk conduction is sufficiently suppressed. On topological insulators *e.g.* Bi_2Se_3[5] and α-Sn,[6] efficient interconversion between spin currents and charge currents was reported at room temperature.

In spintronics studies on TIs, a Bi_2Se_3 family has frequently been used.[7–15] In Bi_2Se_3 systems, bulk-insulating samples are obtained by chemical substitution, *e.g.* Sb substitution in Bi sites and Te substitution in Se sites. However, Bi, Sb, Se, and Te are toxic and volatile. Moreover, to synthesize high-quality TI film samples, high-cost MBE (molecular beam epitaxy) systems have been required; this should be a big barrier to realization of commercial spintronics devices based on TIs. Hence, material search of other topological insulator materials is still important.

In this letter, we focus on a topological intermetallic compound Ru_2Sn_3: a rare strong 3D topological insulator caused by band inversion between Ru $4d$ and Sn $5p$ branches due to strong spin-orbit coupling.[16] Ru_2X_3 (X=Si, Ge, Sn) belongs to a family of Nowotny chimney-ladder compounds.[17,18] Ru_2Si_3 and Ru_2Ge_3 are semiconducting, while metallic resistivity was reported in Ru_2Sn_3[18,19] despite the same number of valence electrons. Band calculations for Ru_2Sn_3 show a small indirect band overlap leading to a semi-metal state,[16,18] while angle-resolved photoemission spectroscopy (APRES) data[16] clearly shows that Ru_2Sn_3 has a full band gap with surface states formed inside the gap. The Fermi energy in the as-prepared Ru_2Sn_3 crystals falls clearly within the bulk band gap,[16] which is suitable for the observation of surface Dirac transport.

Though an ARPES study at 1 K revealed topological surface states of Ru_2Sn_3 near the Fermi level,[16] there has been no follow-up study on the surface properties. Our magnetotransport study on bulk single crystals of Ru_2Sn_3 shows that linear magnetoresistance is observed at low temperatures. Since the linear magnetoresistance emerges in line with a structural phase transition, the present results provide the signature of a linear dispersion in the low-temperature electronic structure. Chemical

doping is thereby not necessary to observe the linear magnetoresistance in Ru_2Sn_3, in contrast to Bi_2Se_3 systems.[2–4] Since Ru and Sn are not so toxic or volatile, and since the non-trivial topological state can be pushed up to room temperature by an applied pressure,[20] Ru_2Sn_3 could be promising for spintronics applications.

The crystal structure of Ru_2Sn_3 at room temperature is illustrated in Fig. 1(a). It is known that Ru_2Sn_3 undergoes a phase transformation from a tetragonal non-centrosymmetric high-temperature structure to an orthorhombic centrosymmetric low-temperature structure.[17,19] At room temperature, Ru_2Sn_3 crystallizes in its tetragonal phase; Ru atoms form a β-Sn type structure with 4-fold helical order along the c axis, and Sn atoms intervene in the voids of the Ru helices and compose another 3-fold helical arrangement along the c axis [Fig. 1(a)].[18] Below room temperature, the atomic displacements occur gradually over a wide temperature range, resulting in the gradual structural phase transition.[17,19] The orthorhombic structure realized in Ru_2Sn_3 at low temperatures is similar to that found in Ru_2Si_3 and Ru_2Ge_3 at room temperature.[17]

Bulk single crystals of Ru_2Sn_3 were grown by a Bi flux method.[16] Powder of Ru (99.95%), Sn (99.99%), and Bi (99.99%) elements was mixed in a molar ratio of Ru : Sn : Bi= 2 : 3 : 67[16] and sealed in an evacuated quartz tube. The powder was then heated up to 800 °C and kept at 800 °C for 12 hours, followed by a slow cooling to 100 °C for 70 hours. Numerous submillimeter-size Ru_2Sn_3 single crystals were obtained by dipping the ingot into dilute HNO_3 acid. Longitudinal and Hall resistivity was measured for a single-crystalline sample being 0.5-mm long, 0.2-mm wide, and 0.05-mm thick. The widest plane was determined to be a (100) plane in the tetragonal phase [Fig. 1(b)]. Electrical contacts were formed by fixing gold wires on the sample using conductive paste. The measurements of magnetoresistance and Hall effects were performed in a 9 tesla Physical Property Measurement System (Quantum Design, Inc.). An external magnetic field was applied perpendicular to the sample plane in the Hall effect measurements, while in the magnetoresistance measurements, the magnetic field direction was changed so that the magnetic field is always perpendicular to the current direction [see Fig. 4(a)].

We show temperature (T) dependence of the longitudinal resistivity, ρ, in Fig. 1(c). ρ increases with decreasing T down to 160 K, and then starts to decrease below 160 K. The temperature dependence of ρ is consistent with the reported one on single crystals[16] and on polycrystals.[18] This unusual
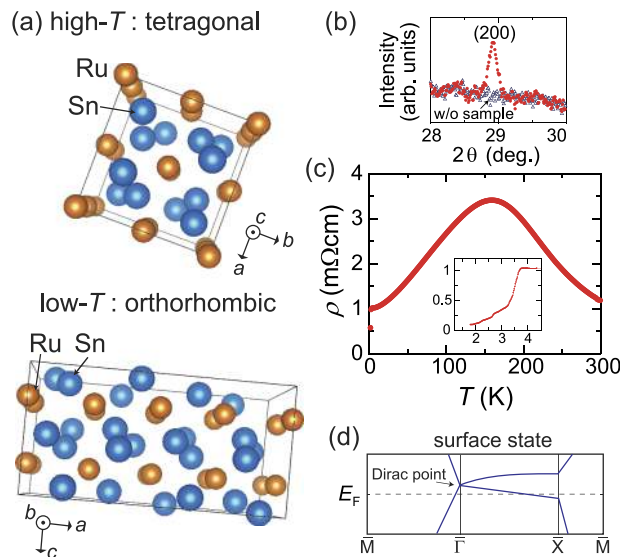

FIG. 1. (a) Schematic illustrations of crystal structures of Ru_2Sn_3 at high and low temperatures. At high temperatures, the tetragonal phase is stable. With decreasing temperature, the gradual phase transition to the orthorhombic phase takes place. (b) θ-2θ scan of the Ru_2Sn_3 sample used in the magnetotransport measurement. A peak corresponding to the [200] direction of the tetragonal phase is observed. (c) Temperature (T) dependence of the resistivity (ρ) without applying magnetic fields. The inset is a magnified view of the low temperature data below 5 K. (d) Schematic of the surface state electronic structure determined by ARPES measurements.[16] E_F denotes the Fermi level.

trend seems to reflect the broad tetragonal to orthorhombic phase transition.[16] Here, it is noted that ρ exhibits a clear drop at 3.7 K, as shown in the inset to Fig. 1(c). This drop is probably due to a superconducting transition of minor Sn-metal contamination observed even in Sn-deficient $Ru_2Sn_{3-\delta}$ samples.[18] Since this superconductivity is limited in a very small T-H region, the impurity phase hardly affects the following magnetotransport studies of Ru_2Sn_3.

Figure 2(a) shows magnetic field (H) dependence of the magnitude of magnetoresistance in perpendicular-to-plane magnetic fields, MR, at various temperatures, where MR is defined as $[\rho(H) - \rho(H=0)]/\rho(H=0)$. In the semiconducting regime above 160 K [Fig. 1(c)], overall H dependence of MR does not change with temperature; the magnetic-field dependence is quadratic, expected in standard conductors. In the metallic regime below 160 K, however, MR starts to increase with decreasing T, as shown in Fig. 2(a). At 5 K, magnetoresistance at high fields is linear with H, and MR reaches 13% at 9 T. Hence, in the metallic regime, the magnetoresistance in the high-field range is linear, not quadratic. The linear MR at low temperatures suggests that the low-T transport is linked to the linear dispersions, as observed in surfaces of topological insulators $(Bi,Sb)_2(Se,Te)_3$[21–25] and SmB_6,[26] Dirac semimetals Cd_3As_2[27–29] and Na_3Bi,[30] and other 3D Dirac materials.[31–33]

In Figs. 3(a) and 3(b), we compare the magnetoresistance at high temperatures [Fig. 3(a)] and at low temperatures [Fig. 3(b)]. As shown in Fig. 3(a), MR above 150 K is quadratic as a function of H in the entire H range from 0 to 9 T. From the quadratic H dependence, the effective mobility, μ_{MR} ($\equiv \sqrt{MR}/\mu_0 H$), is estimated to be 152 cm^2/Vs in the semiconducting region. In the low-T metallic state, by contrast, the magnetoresistance is clearly linear with magnetic fields, as shown in Fig. 3(b). Also remarkable is that, as shown in Fig. 3(c), MR at 9 T suddenly increases below the temperature of $d\rho/dT = 0$, suggesting the enhancement of the mobility in the metallic regime. The large linear magnetoresistance indicates that, with the structural transition from the high-T tetragonal phase to the low-T orthorhombic phase, Dirac fermion transport shows up.

In general, linear magnetoresistance can originate from several mechanisms.[34,35] In the case of linear magnetoresistance in silver chalcogenides $Ag_{2+\delta}Se$ and $Ag_{2+\delta}Te$,[36] multiple scattering by impurities in inhomogeneous conductors is responsible for the giant linear magnetoresistance.[37] On the other hand, linear magnetoresistance can come from quantum effects;[38–40] for gapless semiconductors with a linear energy spectrum, magnetoresistance in perpendicular-to-plane magnetic fields becomes linear with magnetic fields at low temperatures.[41] In recently found topological materials,[21–30] linear magnetoresistance of this mechanism has been observed. In the present case of Ru_2Sn_3, since the linear dispersion of the topological surface state was observed near the Fermi level by ARPES measurements at 1 K,[16] Dirac fermions on the topological surface state may be an origin of the linear magnetoresistance at low temperatures.
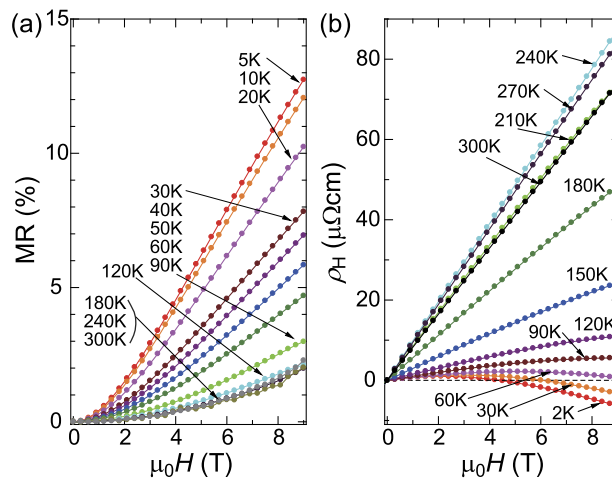

FIG. 2. Magnetic field (H) dependence of (a) the magnitude of magnetoresistance (MR) in perpendicular-to-plane magnetic fields and (b) the Hall resistivity (ρ_H) at various temperatures. Here, MR is defined as $[\rho(H) - \rho(H=0)]/\rho(H=0)$.
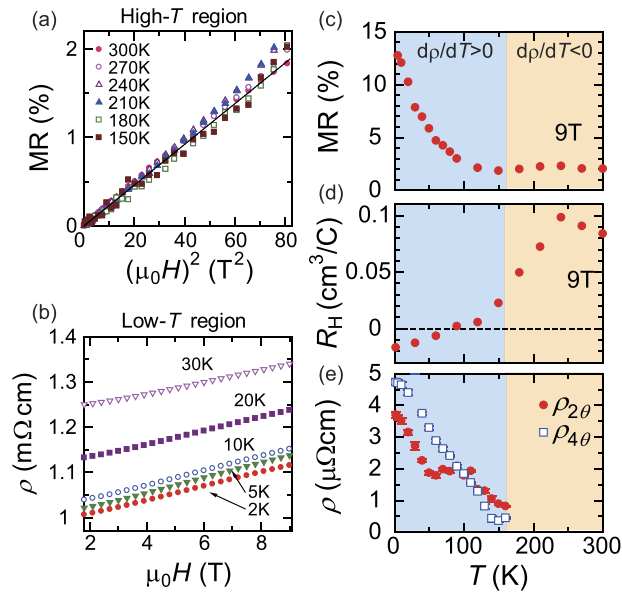
FIG. 3. (a) The magnitude of magnetoresistance (MR) in perpendicular-to-plane magnetic fields as a function of the square of magnetic fields at $T \geq 150$ K. The linear dependence is observed, as indicated by the linear line. (b) Low-temperature longitudinal resistivity (ρ) as a function of magnetic field (H) in $\mu_0 H \gtrsim 2$ T. (c),(d),(e) Temperature (T) dependence of (c) MR at 9 T, (d) the Hall coefficient [$R_H = d\rho_H/d(\mu_0 H)$] at 9 T, and (e) $\rho_{2\theta}$ and $\rho_{4\theta}$ obtained by the fits to the $\rho(\theta)$ data shown in Figs. 4(c) and 4(c). The semiconducting ($d\rho/dT < 0$) and metallic ($d\rho/dT > 0$) regimes are highlighted by different background colors.

To reveal whether the origin of the linear magnetoresistance is 2D or 3D, one standard way is the angular dependence of the magnetoresistance;[22] for 2D surface-state transport, the magnetoresistance will respond only to the perpendicular component of the magnetic field [$H \cos \theta$ in Fig. 4(a)]. Figure 4(b) shows the magnetic-field dependence of ρ at 2 K measured in three field configurations of $\theta = 0°$ (perpendicular-to-plane H), $\theta = 45°$, and $\theta = 90°$ (in-plane H). The overall H dependence of ρ is found to be similar among the different field configurations, which indicates that the linear magnetoresistance is not from 2D surface transport alone but from 3D bulk transport. Though the full-gap bulk state was observed in ARPES measurements,[16] the surface
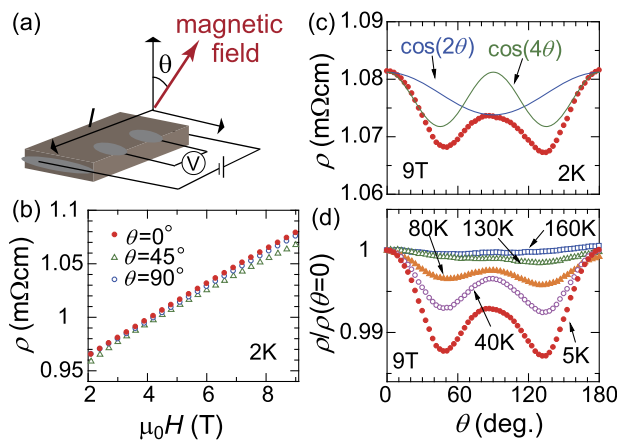

FIG. 4. (a) A schematic illustration of Ru$_2$Sn$_3$ sample contacted by four leads in the magnetoresistance measurement at different tilt angles (θ) between the sample plane and the magnetic field. (b) Magnetic field (H) dependence of ρ at 2 K in three field configurations of $\theta = 0°$, 45°, and 90°. (c) Angular (θ) dependence of ρ measured at 2 K under 9 T. Fitted curves of $\cos(2\theta)$ and $\cos(4\theta)$ components are also shown. (d) Angular (θ) dependence of ρ normalized by ρ at $\theta = 0°$. The angular dependence was measured under 9 T. The data at selected temperatures from 5 K to 160 K are shown.

transport is hardly observed in as-prepared bulk-form samples of Ru_2Sn_3. The situation may be similar to tetradymite topological insulators,[21–25] where sufficiently small bulk volumes[22–24] and/or bulk insulation achieved by bulk carrier compensation[21,25] are necessary to observe the surface conduction.

Though the angle-dependent change in magnetoresistance is as small as 1.5 % at 2 K, the $\rho(\theta)$ exhibits a characteristic angular dependence, as shown in Fig. 4(c). $\rho(\theta)$ has broad peaks around $\theta = 0°$, 90°, and 180°, and dips around $\theta = 45°$ and 135°. Hence, $\rho(\theta)$ seems to include $\cos(2\theta)$ and $\cos(4\theta)$ components. This angle dependence should reflect the anisotropic Fermi surface of Ru_2Sn_3, but looks inconsistent with the star shaped Fermi surface of the topological surface state.[16] As temperature increases, the θ dependences of ρ become smaller, and disappear above 160 K [Fig. 4(d)]. By fits to the $\rho(\theta)$ data at each temperature in the metallic regime, $\rho_{2\theta} \cos(2\theta)$ and $\rho_{4\theta} \cos(4\theta)$ are separated, and the values of $\rho_{2\theta}$ and $\rho_{4\theta}$ are plotted against temperature in Fig. 3(e). $\rho_{2\theta}$ and $\rho_{4\theta}$ are less than 5 $\mu\Omega$cm, which is 1000 times as small as ρ (~ 1 mΩcm).

To further study the magnetotransport properties of Ru_2Sn_3, Hall resistivity, ρ_H, is shown as a function of magnetic fields at various temperatures in Fig. 2(b). In the semiconducting regime above 160 K, the Hall resistivity is positive and linear with magnetic fields. The transport in the semiconducting regime is thereby explained by conduction of thermally-excited holes. From the slope $R_H [\equiv d\rho_H/d(\mu_0 H)]$ at 300 K, the effective carrier density is estimated to be 7.6×10^{19} cm^{-3}. Also, the Hall mobility $(\equiv R_H/\rho)$ at 300 K is 71.1 cm^2/Vs, which is similar to the μ_{MR} value in the high-T range.

As T decreases to the orthorhombic metallic regime, the Hall resistivity clearly deviates from the linear magnetic-field dependence, signaling multi-carrier transport. Below 60 K, the slope R_H at low magnetic fields is still positive, but becomes negative at high magnetic-fields. In a classical expression for Hall effects, the Hall coefficient in the high-field limit reads $1/(en_{eff})$,[42] where n_{eff} is the effective carrier density which includes conduction electrons and holes. In Fig. 3(d), the R_H value at 9 T is shown as a function of T. As T decreases, R_H at 9 T starts to decrease at 240 K and shows a sign change around 100 K. The p-n crossover at low temperatures is in agreement with that observed in the T dependence of the Seebeck coefficient.[16]

The electron carriers which dominate low temperature transport are expected to induce the linear magnetoresistance in the metallic regime [Fig. 3(b)]. In fact, in Figs. 3(c) and 3(d), the rapid increase in MR is observed at low temperatures where the sign of R_H is negative. Though the Dirac dispersion of the topological surface state was observed near the Fermi level,[16] the topological surface state is unlikely to produce electron carriers; in an ARPES measurement,[16] a single Dirac point originating from the band inversion is located above the Fermi level at $\bar{\Gamma}$ [Fig. 1(d)],[16] which implies hole conduction on the surface states. The small θ dependence of linear magnetoresistance [Fig. 4(b)] also supports that the linear magnetoresistance results from the 3D bulk transport, whereas a linear dispersion has not been reported in the bulk electronic structure.[16] Nevertheless, an expected semimetallic or narrow-gap semiconducting bulk-state is suitable for the observation of quantum linear magnetoresistance, if it has small pockets of the Fermi surface with a small effective mass.[43] Since there is discrepancy between calculated electronic structure[16,18] and ARPES data,[16] future in-depth calculations are required for the full understanding of the magnetotransport results.

In summary, magnetoresistance and Hall effects were studied in a topological insulator Ru_2Sn_3. Magnetotransport properties are dramatically different between the high-temperature tetragonal phase and the low-temperature orthorhombic phase. Magnetoresistance shows classical quadratic magnetic-field dependence in the high-temperature semiconducting regime, while it becomes linear in the low-temperature metallic regime. As opposed to the reported data on the surface electronic structure near the Fermi level,[16] the linear magnetoresistance at low temperatures seems to originate from the linear-like dispersion in the bulk state. In the Hall-effect measurement, a p-n crossover of dominant carriers was observed with decreasing temperature, which suggests that the electron carriers are expected to induce the linear magnetoresistance. In contrast to the tetradymite topological insulators, nanofabrication or bulk-carrier compensation is not necessary to observe linear magnetoresistance in Ru_2Sn_3, which may be promising for application in topological spintronics.

[1] W. Han, R. K. Kawakami, M. Gmitra, and J. Fabian, Nature Nanotech. **9**, 794–807 (2014).

[2] Y. Ando, J. Phys. Soc. Jpn. **82**, 102001 (2013).

[3] M. Z. Hasan and C. L. Kane, Rev. Mod. Phys. **82**, 3045–3067 (2010).

[4] X.-L. Qi and S.-C. Zhang, Rev. Mod. Phys. **83**, 1057–1110 (2011).

[5] A. R. Mellnik, J. S. Lee, A. Richardella, J. L. Grab, P. J. Mintun, M. H. Fischer, A. Vaezi, A. Manchon, E.-A. Kim, N. Samarth, and D. C. Ralph, Nature **511**, 449–451 (2014).

[6] J.-C. Rojas-Sanchez, S. Oyarzun, Y. Fu, A. Marty, C. Vergnaud, S. Gambarelli, L. Vila, M. Jamet, Y. Ohtsubo, A. Taleb-Ibrahimi, P. Le Fevre, F. Bertran, N. Reyren, J.-M. George, and A. Fert, Phys. Rev. Lett. **116**, 096602 (2016).

[7] Y. Fan, P. Upadhyaya, X. Kou, M. Lang, S. Takei, Z. Wang, J. Tang, L. He, L.-T. Chang, M. Montazeri, G. Yu, W. Jiang, T. Nie, R. N. Schwartz, Y. Tserkovnyak, and K. L. Wang, Nature Mater. **13**, 699–704 (2014).

[8] A. A. Baker, A. I. Figueroa, L. J. Collins-McIntyre, G. van der Laan, and T. Hesjedal, Sci. Rep. **5**, 7907 (2015).

[9] P. Deorani, J. Son, K. Banerjee, N. Koirala, M. Brahlek, S. Oh, and H. Yang, Phys. Rev. B **90**, 094403 (2014).

[10] M. Jamali, J. S. Lee, J. S. Jeong, F. Mahfouzi, Y. Lv, Z. Zhao, B. K. Nikolic, K. A. Mkhoyan, N. Samarth, and J.-P. Wang, Nano Lett. **15**, 7126–7132 (2015).

[11] Y. Shiomi, K. Nomura, Y. Kajiwara, K. Eto, M. Novak, K. Segawa, Y. Ando, and E. Saitoh, Phys. Rev. Lett. **113**, 196601 (2014).

[12] Y. Ando, T. Hamasaki, T. Kurokawa, K. Ichiba, F. Yang, M. Novak, S. Sasaki, K. Segawa, Y. Ando, and M. Shiraishi, Nano Lett. **14**, 6226–6230 (2014).

[13] H. Wang, J. Kally, J. S. Lee, T. Liu, H. Chang, D. R. Hickey, K. A. Mkhoyan, M. Wu, A. Richardella, and N. Samarth, Phys. Rev. Lett. **117**, 076601 (2016).

[14] Y. Wang, P. Deorani, K. Banerjee, N. Koirala, M. Brahlek, S. Oh, and H. Yang, Phys. Rev. Lett. **114**, 257202 (2015).

[15] K. Kondou, R. Yoshimi, A. Tsukazaki, Y. Fukuma, J. Matsuno, K. S. Takahashi, M. Kawasaki, Y. Tokura, and Y. Otani, Nat. Phys. **12**, 1027–1031 (2016).

[16] Q. D. Gibson, D. Evtushinsky, A. N. Yaresko, V. B. Zabolotnyy, M. N. Ali, M. K. Fuccillo, J. Van den Brink, B. Buchner, R. J. Cava, and S. V. Borisenko, Sci. Rep. **4**, 5168 (2014).

[17] D. J. Poutcharovsky, K. Yvon, and E. Parthé, J. Less-Common Met. **40**, 139 (1975).

[18] H. Kawasoko, T. Takayama, and H. Takagi, Appl. Phys. Express **7**, 115801 (2014).

[19] C. P. Susz, J. Muller, K. Yvon, and E. Parthé, J. Less-Common Met. **71**, P1–P8 (1980).

[20] S. Zhang, Q. D. Gibson, W. Yi, J. Guo, Z. Wang, Y. Zhou, H. Wang, S. Cai, K. Yang, A. Li, Q. Wu, R J Cava, L. Sun, Z. Zhao, arXiv:1612.05385 (2016).

[21] D.-X. Qu, Y. S. Hor, J. Xiong, R. J. Cava, and N. P. Ong, Science **329**, 821–824 (2010).

[22] H. Tang, D. Liang, R. L. J. Qiu, and X. P. A. Gao, ACS Nano **5**, 7510 (2011).

[23] H. He, B. Li, H. Liu, X. Guo, Z. Wang, M. Xie, and J. Wang, Appl. Phys. Lett. **100**, 032105 (2012).

[24] S. X. Zhang, R. D. McDonald, A. Shekhter, Z. X. Bi, Y. Li, Q. X. Jia, and S. T. Picraux, Appl. Phys. Lett. **101**, 202403 (2012).

[25] W. Wang, W. Q. Zou, L. He, J. Peng, R. Zhang, X. S. Wu, and F. M. Zhang, J. Phys. D: Appl. Phys. **48**, 205305 (2015).

[26] S. Thomas, D. J. Kim, S. B. Chung, T. Grant, Z. Fisk, and J. Xia, Phys. Rev. B **94**, 205114 (2016).

[27] L. P. He, X. C. Hong, J. K. Dong, J. Pan, Z. Zhang, J. Zhang, and S. Y. Li, Phys. Rev. Lett. **113**, 246402 (2014).

[28] A. Narayanan, M. D. Watson, S. F. Blake, N. Bruyant, L. Drigo, Y. L. Chen, D. Prabhakaran, B. Yan, C. Felser, T. Kong, P. C. Canfield, and A. I. Coldea, Phys. Rev. Lett. **114**, 117201 (2015).

[29] T. Liang, Q. Gibson, M. N. Ali, M. Liu, R. J. Cava, and N. P. Ong, Nature Mater. **14**, 280–284 (2015).

[30] S. K. Kushwaha, J. W. Krizan, B. E. Feldman, A. Gyenis, M. T. Randeria, J. Xiong, S.-Y. Xu, N. Alidoust, I. Belopolski, T. Liang, M. Z. Hasan, N. P. Ong, A. Yazdani, and R. J. Cava, APL Mater. **3**, 041504 (2015).

[31] K. Wang, D. Graf, H. Lei, S. W. Tozer, and C. Petrovic, Phys. Rev. B **84**, 220401 (2011).

[32] K. Wang and C. Petrovic, Phys. Rev. B **86**, 155213 (2012).

[33] X. Z. Xing, C. Q. Xu, N. Zhou, B. Li, J. Zhang, Z. X. Shi, and X. Xu, Appl. Phys. Lett. **109**, 122403 (2016).

[34] M. Veldhorst, M. Snelder, M. Hoek, C. G. Molenaar, D. P. Leusink, A. A. Golubov, H. Hilgenkamp, and A. Brinkman, Phys. Status Solidi RRL **7**, 26–38 (2013).

[35] J. Hu and T. F. Rosenbaum, Nature Mater. **7**, 697–700 (2008).

[36] M. M. Parish and P. B. Littlewood, Nature **426**, 162–165 (2003).

[37] N. V. Kozlova, N. Mori, O. Makarovsky, L. Eaves, Q. D. Zhuang, A. Krier, and A. Patanè, Nat. Commun. **3**, 1097 (2012).

[38] A. A. Abrikosov, JETP **29**, 746–753 (1969).

[39] A. A. Abrikosov, Phys. Rev. B **58**, 2788–2794 (1998).

[40] A. A. Abrikosov, Europhys. Lett. **49**, 789–793 (2000).

[41] Y. Shiomi and E. Saitoh, Sci. Rep. **6**, 22085 (2016).

[42] See, for example, *Semiconductors*, edited by R. A. Smith (Cambridge University Press, Cambridge, England, 1978).

[43] J. Hu and T. F. Rosenbaum, Nature Mater. **7**, 697–700 (2008).